



29 conductance is about 8.5 TgO₃, while using a dynamic layer that ensures plants to maximize the water
30 uptake from soil, we found a reduction of about 10% in the amount of ozone removed by dry
31 deposition (~7.7 TgO₃). Despite dry deposition occurs from top of canopy to ground level, it affects the
32 concentration of gases remaining into the lower atmosphere with a significant impact on ozone
33 concentration (up to 4 ppb) extending from the surface to the upper troposphere (up to 650 hPa).
34 Our results shed light on the importance of improving the parameterizations of processes occurring at
35 plant level (i.e. from the soil to the canopy) as they have significant implications on concentration of
36 gases in the lower troposphere.

37

38 1. Introduction

39 Plant-level water cycling and exchange of air pollutants between atmosphere and vegetation are
40 intimately coupled (Eamus, 2003; Domec et al., 2010), thus any factor affecting root water absorption
41 by plants is expected to impact the concentration of gases in the lower troposphere by changing
42 deposition rates. In fact, atmospheric gases, including air pollutants, are primarily removed from the
43 troposphere by dry deposition to the Earth's surface (Hardacre et al., 2015; Monks et al., 2015). A
44 major part of dry deposition to vegetation is regulated by stomata opening which strongly depends on
45 the amount of water available in the soil (Büker et al., 2012). Therefore a proper quantification of soil
46 water content as well as a proper understanding of stomatal response to soil moisture are required for
47 correctly quantifying the concentration of gases in the atmosphere, particularly in water-limited
48 ecosystems (dry and semidry environments) which cover 41% of Earth's land surface (Reynolds et al.,
49 2007).

50 Among common air gasses, ozone (O₃) plays a pivotal role in the Earth system: in fact, it affects
51 climate with a direct radiative forcing of 0.2-0.6 W m⁻² (Shindell et al., 2009, 2012; Ainsworth et al.,
52 2012; Myhre et al., 2013) and the ecosystems, causing a reduction of carbon assimilation by vegetation
53 (Wittig et al., 2009) that accelerates the rate of rise in CO₂ concentrations with indirect implications for
54 climate change (Sitch et al., 2007). In addition, O₃ accelerates leaf senescence (Gielen et al., 2007),
55 changes plants susceptibility to abiotic and biotic stress factors (Karnosky et al., 2002) and makes
56 sluggish or impaired response of stomata to environmental stimuli (Hoshika et al., 2015).

57 At European level, the model currently parameterized for European vegetation and developed to
58 estimate surface O₃ fluxes is the DO₃SE (Deposition of O₃ and Stomatal Exchange) model (Emberson
59 et al., 2000); it is widely used embedded within chemistry transport models (CTMs) (Tuovinen et al.,
60 2004; Simpson et al., 2007,2012; Menut et al., 2013) to estimate dry deposition rates as well as stand-



61 alone for O₃ risk assessment (Emberson et al., 2007; Tuovinen et al., 2009; Klingberg et al., 2014;
62 Anav et al., 2016; Sicard et al., 2016; Karlsson et al., 2017). The DO₃SE model is based on the
63 multiplicative Jarvis' algorithm for calculation of stomatal conductance (Jarvis 1976), which integrates
64 the effects of multiple climatic factors, vegetation characteristics and local features (Emberson et al.,
65 2000). The leaf-level stomatal conductance is estimated considering the variation in the maximum
66 stomatal conductance (g_{\max}) with photosynthetic photon flux density, surface air temperature, and
67 vapour pressure deficit. However, this original formulation of the DO₃SE model presented a main
68 limitation (Simpson et al., 2007; Tuovinen et al., 2009; Mills et al., 2011): for both forests and crops
69 the model did not take into account the limitation due to soil water content. This approach ensured that
70 stomatal fluxes were maximized, corresponding to conditions expected for irrigated areas (Simpson et
71 al., 2007), but, in semi-arid environments, like the Mediterranean basin, the amount of atmospheric
72 gases entering the leaves might be compromised by the exclusion of the influence of drought on
73 stomatal conductance (Tuovinen et al., 2009; Mills et al., 2011; Bükér et al., 2012; Anav et al., 2016;
74 De Marco et al., 2016). Following this assumption, the role of soil moisture on stomatal O₃ fluxes has
75 been often neglected in risk assessment studies because soil water is very difficult to model accurately
76 in large-scale models, as it depends on parameters (such as soil texture, vegetation characteristics and
77 rooting depth) that are not easily available in the frame of large scale models (Simpson et al., 2007;
78 Bükér et al., 2012; Simpson et al., 2012).

79 However, in the last decade the importance of soil water stress on vegetation has been well
80 demonstrated in several studies reporting a large reduction in the amount of air gases up-taken from the
81 atmosphere during heat waves or drought years (e.g. Ciais et al., 2005; Granier et al., 2007; Reichstein
82 et al., 2007) with species responding in different ways to scarce water availability, depending on eco-
83 hydrological properties (Granier et al., 1996; Pataki et al., 2000; Pataki and Oren, 2003) and drought
84 avoidance and tolerance strategies (Martinez-Ferri et al., 2000; Bolte et al., 2007). For instance,
85 drought-avoiding species (e.g. *Pinus spp.*) prevent damage by an early stomatal closure that leads to a
86 sharp carbon assimilation inhibition, whereas drought-tolerant species (e.g. *Quercus spp.*) exhibit a
87 simultaneous decrease in stomatal conductance and water potential (Guehl et al., 1991, Picon et al.,
88 1996) that does not significantly limit carbon assimilation. Nevertheless, both strategies have severe
89 implications on the concentration of gases in the lower troposphere.

90 Moreover, it is important to take into account that soil drying does not occur at the same rate at
91 different depths, and the drying rate is more pronounced in the superficial soil layers than in the deeper
92 ones. Overall, deep-rooted forest systems take up water from deep to shallow soil horizons (Aranda et



93 al., 2012). In contrast, shallow-rooted grass normally adsorbs available soil water from top–middle
94 soil, while shrubs can take up soil water adaptively from top to deep soil layers, with increased use of
95 top-soil water under non-drought stress and a tendency of using water from deeper soil under drought
96 stress (Wu et al., 2017). Thus, plants able to develop a deeper root system usually are more tolerant to
97 low water availability than plants with a more superficial root system (Canadell et al., 1996). Jackson
98 et al. (2000) showed that differences in rooting depth patterns vary between world's major plant
99 biomes, with plants of xeric environments having deeper root-depth distributions than plants in more
100 humid environments. In contrast, Schenk and Jackson (2002) found that maximum rooting depths tend
101 to be shallowest in arid regions and deepest in sub-humid regions.

102 Consequently, the role of root systems is fundamental in stomatal conductance regulation and thus in
103 atmospheric chemistry modeling. For these reasons, recently the DO₃SE model has been improved to
104 account for the soil moisture limitation to stomatal conductance (Büker et al., 2012; Simpson et al.,
105 2012).

106 Chemistry transport models are widely used to estimate the concentration of gases in atmosphere at
107 both regional and global scale; in these models the concentration of a given gas-species is mainly
108 regulated and parameterized by three different processes: atmospheric transport, chemical
109 production/destruction and losses to surface by dry deposition (Monks et al., 2015). Within these
110 models, the dry deposition is generally simulated through an electrical resistance analogy (Wesely
111 1989; Monk et al., 2015), namely the transport of material to the surface is assumed to be controlled by
112 three different resistances: the aerodynamic resistance (R_a), the quasi-laminar layer resistance (R_b), and
113 the surface resistance (R_c). The surface resistance is regulated by the stomatal uptake, which relies on
114 stomatal conductance, as well as external plant surfaces like the soil underlying the vegetation.

115 In this study, we improve the dry deposition scheme within the chemistry transport model CHIMERE
116 considering the effect of soil water limitation to stomatal conductance. Our main aim was to perform
117 several different simulations testing various hypotheses of water uptake by plants at different soil
118 depths in the rooting zone, based on the main assumption that roots maximize water uptake to fulfill
119 resource requirements adsorbing water at different depths depending on the water availability. Finally
120 we show and discuss the resulting effects on O₃ dry deposition and concentration, in order to stress the
121 need of a proper parameterization of root-depth soil moisture when evaluating the stomatal feedbacks
122 on the atmosphere and for a thorough O₃ risk assessment.

123

124



125 2. Methodology

126 2.1. The multi-model framework

127 We use a multi-model system to reproduce the meteorological conditions and the concentration of
128 gases in the troposphere; this framework is composed by the WRF (Weather Research and Forecast
129 Model) regional meteorological model and the CHIMERE chemistry-transport model.

130 In this study, in order to have a large latitudinal gradient and assess the role of soil moisture across
131 different climate zones, we selected a domain extending over all Europe (except Iceland). For both
132 WRF and CHIMERE we performed a simulation for the whole year 2011, with a spin up of 2 months
133 to initialize all the fields.

134

135 2.1.1. The meteorological model WRF

136 Meteorological variables are simulated with the WRF regional model (v 3.6); it is a limited-area,
137 non-hydrostatic, terrain-following eta-coordinate mesoscale model (Skamarock et al., 2008) widely
138 used worldwide for climate studies. In our configuration, the model domain is projected on a regular
139 latitude-longitude grid with a spatial resolution of 16 km and with 30 vertical levels extending from
140 land surface to 50 hPa. The initial and boundary meteorological conditions required to run the WRF
141 model are provided by the European Centre for Medium-range Weather Forecast (ECMWF) analyses
142 with a horizontal resolution of 0.7° every 6 hours (Dee et al., 2011).

143 The exchange of heat, water and momentum between soil-vegetation and atmosphere is calculated
144 using the Noah land surface model (Chen and Dudhia, 2001); in our configuration the soil has a
145 vertical profile with a total depth of 2 m below the surface and it is partitioned into four layers with
146 thicknesses of 10, 30, 60, and 100 cm (giving a total of 2 m). The root zone is fixed at 100 cm (i.e.
147 including the top three soil layers). Thus, the lower 100 cm of soil layer acts as a reservoir with gravity
148 drainage at the bottom (Al-Shrafany et al., 2013).

149 For each soil layer Noah calculates the volumetric soil water content (θ) from the mass conservation
150 law and the diffusivity form of Richards' equation (Chen and Dudhia, 2001):

151

$$152 \quad \frac{\partial \theta}{\partial t} = \frac{\partial \theta}{\partial z} \left(D \frac{\partial \theta}{\partial z} \right) + \frac{\partial K}{\partial z} + F_{\theta} \quad (1)$$

153 where D is the soil water diffusivity, K is the hydraulic conductivity, F_{θ} represents additional sinks and
154 sources of water (i.e., precipitation, evaporation and runoff), t is time and z is the soil layer depth



155 (Chen and Dudhia, 2001; Al-Shrafany et al., 2013; Greve et al., 2013). Integrating Eq. (1) over four
 156 soil layers and expanding F_0 , we can calculate the volumetric soil water content for each soil layer
 157 (Chen and Dudhia, 2001; Al-Shrafany et al., 2013):

158

$$159 \quad d_{z1} \frac{\partial \theta_1}{\partial t} = -D \left(\frac{\partial \theta}{\partial z} \right)_{z1} - K_{z1} + P_d - R - E_{dir} - E_{r1} \quad (2)$$

$$160 \quad d_{z2} \frac{\partial \theta_2}{\partial t} = D \left(\frac{\partial \theta}{\partial z} \right)_{z1} - D \left(\frac{\partial \theta}{\partial z} \right)_{z2} + K_{z1} - K_{z2} - E_{r2} \quad (3)$$

$$161 \quad d_{z3} \frac{\partial \theta_3}{\partial t} = D \left(\frac{\partial \theta}{\partial z} \right)_{z2} - D \left(\frac{\partial \theta}{\partial z} \right)_{z3} + K_{z2} - K_{z3} - E_{r3} \quad (4)$$

$$162 \quad d_{z4} \frac{\partial \theta_4}{\partial t} = D \left(\frac{\partial \theta}{\partial z} \right)_{z3} + K_{z3} - K_{z4} \quad (5)$$

163

164 where, d_{zi} is the thickness of the i th soil layer, P_d is the precipitation not intercepted by the canopy, E_{ti}
 165 represents the canopy transpiration taken by the canopy root in the i th layer within the root zone, E_{dir} is
 166 the direct evaporation from the top surface soil layer, and R is the surface runoff, calculated using the
 167 Simple Water Balance (SWB) model (Schaake et al., 1996). In the deeper soil layer (i.e. 4th) the
 168 hydraulic diffusivity is assumed to be zero, so that the soil water flux is due only to the gravitational
 169 percolation term K_{z4} (i.e. drainage). A full and detailed description of the above mentioned
 170 parameterizations used by the Noah scheme can be found in Chen and Dudhia (2001).

171 For the definition of vegetation and land cover WRF uses the United States Geological Survey (USGS)
 172 land cover dataset, which has a resolution of 1km with 24 categories (Loveland et al., 2000; Hibbard et
 173 al., 2010; Sertel et al., 2010); this land cover dataset is derived from the 1 km satellite Advanced Very
 174 High Resolution Radiometer (AVHRR) data. In addition to land cover, WRF defines 12 soil types and
 175 four non-soil types, including organic material, water, bedrock, and ice. Soil types are classified based
 176 on the percentage of sand, silt, and clay in the soil (Dy and Fung, 2016); for each soil type, WRF has a
 177 default soil parameter table that generalizes the hydraulic and thermal properties of the soil. Soil
 178 texture data are derived from the 5-minute Food and Agriculture Organization's (FAO) 16 categories
 179 soil types.

180 One useful capability of WRF is its flexibility in choosing different dynamical and physical schemes;
 181 **Table 1** lists the main options used in this study for physical schemes.

182



183

Table 1. WRF 3.6 physical configurations used in the model simulations.

Process	Configuration	Reference
Microphysics	Single Moment-3 class (mp_physics = 3)*	Hong <i>et al.</i> (2004)
Cumulus Parameterization	Kain–Fritsch (cu_physics = 1)*	Kain (2004)
Shortwave Radiation	RRTM (ra_sw_physics = 1)*	Mlawer <i>et al.</i> (1997)
Longwave Radiation	RRTM (ra_lw_physics = 1)*	Mlawer <i>et al.</i> (1997)
Land-surface	Noah land model (sf_surface_physics = 2)*	Chen and Dudhia (2001)
Planetary Boundary Layer	YSU (bl_pbl_physics = 1)*	Hong <i>et al.</i> (2006)

184 *A complete description of parameterizations and model's flags is given in the WRF 3 user guide
 185 (http://www2.mmm.ucar.edu/wrf/users/docs/user_guide_V3.6/ARWUsersGuideV3.6.1.pdf)

186

187 2.1.2. The chemistry-transport model CHIMERE

188 The chemistry transport model used in this study is CHIMERE (v2014b), an Eulerian model developed
 189 to simulate gas-phase chemistry, aerosol formation, transport and deposition at regional scale (Menut
 190 *et al.*, 2013).

191 The gas-phase chemical mechanism used by CHIMERE is MELCHIOR2 (Lattuati, 1997), which
 192 consists of a simplified version (40 chemical species, 120 reactions) of the full chemical mechanism
 193 MELCHIOR; this latter describes more than 300 reactions of 80 species. Photolysis rates are explicitly
 194 calculated using the FastJ radiation module (Wild *et al.*, 2000), as described by Mailler *et al.* (2016;
 195 2017). External meteorological forcing required by CHIMERE to calculate the atmospheric
 196 concentrations of gas-phase and aerosol species are directly provided by the WRF simulation. In
 197 addition, to accurately reproduce the gas-phase chemistry, emissions must be provided every hour for
 198 the specific species of the chemical mechanism. For studies over Europe, the EMEP inventory
 199 (Vestreng *et al.*, 2009) is usually used for anthropogenic emissions of NO_x, CO, SO₂, PM_{2.5} and PM₁₀.
 200 Biogenic emissions of six species (isoprene, α -pinene, β -pinene, limonene, ocimene, and NO) are
 201 calculated through the MEGAN model (Guenther *et al.*, 2006). This model parameterizes the bulk
 202 effect of changing environmental conditions using three time-dependent input variables: surface air
 203 temperature, radiation and foliage density (i.e. LAI). In the standard version of CHIMERE, LAI
 204 database is given as a monthly mean product derived from MODIS observations, referred to base year
 205 2000 (Menut *et al.*, 2013). However, as climate change leads to a widespread greening of Earth surface
 206 (Zhu *et al.*, 2016), a mean climatological LAI referred to year 2000 could not be adequate to correctly
 207 simulate biogenic emissions during our simulation (year 2011). Thus, here we replaced the original
 208 LAI data with mean monthly GIMMS-LAI3g data (Zhu *et al.*, 2013) for the year 2011.



209 Boundary conditions are provided as a monthly climatology of the LMDz-INCA global chemistry-
210 transport model (Hauglustaine et al., 2004; Folberth et al., 2006) for gaseous species and the GOCART
211 model (Ginoux et al., 2001) for aerosol species. More details regarding the parameterizations of the
212 above mentioned processes are described in Menut et al. (2013).

213

214 **2.1.3. Dry deposition: the DO₃SE model**

215 The leaf-level stomatal conductance is estimated by CHIMERE using the DO₃SE model (Emberson et
216 al., 2000). As already introduced above, this model integrates the effects of multiple climatic factors,
217 vegetation characteristics and local features through some limiting functions (e.g. Emberson et al.,
218 2000). The limiting functions consider the variation in the maximum stomatal conductance (g_{max}) with
219 photosynthetic photon flux density (f_{light}), surface air temperature (f_{temp}) and vapour pressure deficit
220 (f_{VPD}) (Mills et al., 2011; Büker et al., 2012); they vary between 0 and 1, with 1 meaning no limitation
221 to stomatal conductance (e.g. Emberson et al., 2000; Mills et al., 2011). In addition, the DO₃SE model
222 requires another function describing the phenology of vegetation (f_{phen}); this function is used to
223 compute the duration of growing season during which plants can uptake gases from atmosphere (Anav
224 et al., 2017).

225 Here, we improve the DO₃SE scheme within CHIMERE considering also the soil water content (SWC)
226 limitation to stomatal conductance; the soil-water limitation function is defined as:

227

$$228 \quad f_{SWC} = \min \left[1, \max \left(f_{min}, \frac{SWC - WP}{FC - WP} \right) \right] \quad (6)$$

229 where WP and FC are the soil water content at wilting point and at field capacity, respectively; these
230 two parameters are constant and depend on the soil type. Given the above-mentioned limiting
231 functions, the stomatal conductance is computed as following:

232

$$233 \quad g_{sto} = g_{max} * f_{phen} * f_{light} * \max(f_{min}, f_{temp} * f_{VPD} * f_{SWC}) \quad (7)$$

234

235 where g_{max} is the maximum stomatal conductance of a plant species to O₃ and f_{min} is the minimum
236 stomatal conductance expressed as a fraction of g_{max} (Emberson et al., 2000).



237 Meteorological fields required by the DO₃SE model, such as 2m air temperature, relative humidity,
238 short wave radiation and soil moisture, are directly provided by WRF. As already discussed above,
239 WRF computes soil moisture over four soil layers of different thicknesses. For the integrated risk
240 assessment studies, some authors make use of 1m soil layer to compute the stomatal O₃ flux and dry-
241 deposition (e.g. Simpson et al., 2012), while other authors use a shallower soil moisture layer (e.g. De
242 Marco et al., 2016) as most of the absorbing fine roots concentrate in the top soil layer (Jackson et al.,
243 1996; Vinceti et al., 1998). Here we perform five different simulations testing various hypotheses: 1)
244 no soil moisture limitation to stomatal conductance (henceforth *NO_SWC*), 2) soil moisture from first
245 soil layer (i.e. 0-10 cm depth, henceforth *SWC_10cm*), 3) soil moisture from middle soil (i.e., 10-40 cm
246 depth, henceforth *SWC_40cm*), 4) soil moisture from the deeper soil layer of rooting zone (i.e., 0.4-1 m
247 depth, henceforth *SWC_1m*) and 5) a dynamic layer (henceforth *SWC_DYN*) supporting the hypothesis
248 that plants adsorb water at the depth with the higher water content availability.

249 As the original version of CHIMERE does not account for any limitation of soil moisture to stomatal
250 conductance, in the following analysis we use the simulation *NO_SWC* as reference; thus we show and
251 discuss models' changes with respect to this original configuration (Menut et al., 2013).

252

253 **2.2. Measurement data and statistical analysis**

254 In order to assess how the new parameterization of dry deposition changes the ability of CHIMERE to
255 reproduce the spatial distribution of surface O₃ concentration, we compare the simulated data at
256 surface level against in-situ measurements. Station data were obtained from the European air quality
257 database (AirBase) and maintained by the European Environment Agency (EEA)
258 (<http://acm.eionet.europa.eu/databases/airbase/>).

259 For the validation of O₃ bias, computed comparing hourly simulated O₃ concentrations with AirBase
260 data, we use the root-mean-square error (RMSE), while to assess the agreement in the phase (i.e.
261 hourly cycle) we use the correlation coefficient.

262 Considering the soil moisture, we retrieve precipitation data over four forested eddy covariance sites
263 belonging to the European flux network (<http://www.europe-fluxdata.eu>); in fact, a good representation
264 of precipitation simulated by the model is mandatory to correctly reproduce the dynamics of water in
265 the soil. The choice of these specific sites is due to the multiple requirements of having full year data
266 coverage with different climatic zones. Specifically, the sites cover a continental climate typical of
267 central Europe, where soil moisture barely limits the stomatal opening, and Mediterranean sites
268 characterized by scarce water availability during summer months. Unfortunately, despite soil moisture



269 is measured in these sites, the depth of measurements is not consistent with model's layers and also it
270 does not reach the same depth of the model making thus awkward any comparison of the vertical
271 distribution of water in the soil.

272

273 3. Results

274 3.1. Seasonal changes in soil water content

275 **Figure 1** shows the seasonal variation of simulated soil water content at four different locations; in
276 order to assess the reliability of vertical soil moisture profiles we also evaluate models skills in
277 capturing precipitation events by comparing the simulated precipitation with data collected over the
278 four measurements stations.

279 The first site, Leinefelde in Germany, is characterized by a temperate/continental climate with mean
280 annual precipitation ranging between 700 and 750 mm, covered by a beech forest (*Fagus sylvatica*).
281 Overall, compared to in-situ observations, WRF well reproduces both the rainfall events and their
282 intensity (**Figure 1a**). Considering the soil moisture, at the beginning of the year, the soil is at field
283 capacity, and rapidly becomes saturated down to 40 cm, while below 1m depth from end of January to
284 mid-April the soil is close to the field capacity. After mid-April, soil remarkably dries out at all depths,
285 and water content oscillates between 0.28 and 0.36 m³·m⁻³ until October, when decreasing evaporative
286 demand and weak rain events caused a transient partial recovery around 0.33 m³·m⁻³. Then, the new
287 rainfall events at the end of November lead to rising soil water content above the field capacity until
288 the end of the year (**Figure 1a**).

289 The second temperate site, covered by a spruce forest (*Picea abies*), is Oberbärenburg in Germany; it is
290 characterized by a mean annual precipitation of about 1000 mm. Noteworthy, WRF captures most of
291 the rainfall events, despite it slightly underestimates their intensity during the period May-August.
292 Here, in the rooting zone, the soil is constantly above the field capacity and near saturation until mid-
293 March; then it rapidly drains, and soil water content remains in the range 0.24–0.26 m³·m⁻³, with short-
294 term increases following precipitation events, until December, when it increased to above 0.28 m³·m⁻³
295 (**Figure 1b**).

296 In Collelongo, a *Fagus sylvatica* mountain forest site in central Italy, the mean annual precipitation is
297 about 1200 mm. From the beginning of the year to the end of June, the soil water content is above 0.3
298 m³·m⁻³, with short term increases above field capacity from 10 cm to 1m and a stable content above
299 field capacity below 1m depth; then, in July, soil moisture progressively decreases to about 0.20 m³·m⁻³
300 ³ with a short term rainfall resupply at the end of the month. From August to November, because of



301 high evapotranspiration rates and weak precipitation events, soil moisture sharply drops to $0.15 \text{ m}^3\cdot\text{m}^{-3}$
302 or less, and, at 1m depth, it appears to have been constantly at wilting point from end of September to
303 early November. Finally, in December, soil moisture rapidly increases in the upper layers, reaching
304 near saturation in late December, but remains low around 1m depth until the end of the year (**Figure**
305 **1c**).

306 The fourth station is San Rossore, a Mediterranean *Pinus spp.* forest located on the coastal region of
307 central Italy and characterized by a mean annual precipitation of 920 mm. Here the pattern is
308 substantially similar to Collelongo: soil water content is lower in spring, when rainfall infiltrates faster
309 and deeper and less water is retained; the fall drought at 1m depth is less pronounced and of shorter
310 duration, but water recharge towards the end of the year was again slower (**Figure 1d**).

311 Overall, these results suggest that soil water availability was higher from April to September for the
312 two Central European sites, where soil water content remained above 50% of total available water
313 capacity. In the Mediterranean sites, water availability declined from spring onwards, but remained
314 above 40% total available water capacity until late August, while effective drought conditions occurred
315 in October.

316

317 **3.2. Changes in O₃ dry deposition**

318 The inclusion of soil water limitation in the stomatal conductance parameterization affects, at first, the
319 surface resistance, that, in turn, affects the dry deposition velocity and thus the amount of air pollutants
320 removed from the surface layer by dry deposition (Seinfeld and Pandis, 2016; Hardacre et al., 2015;
321 Monks et al., 2015). **Figure 2** shows the mean percentage of change in O₃ dry deposition during the
322 periods April-May-June (AMJ) and July-August-September (JAS) between the reference simulation
323 (i.e. *NO_SWC*) and the simulations that take into account the soil moisture limitation to stomatal
324 conductance. Clearly, as the inclusion of soil water stress leads to a reduction of stomatal conductance,
325 the amount of O₃ removed by dry deposition is always larger in the *NO_SWC* simulation than in the
326 other simulations; this explains the negative pattern in the percentage of change in O₃ dry deposition in
327 both the analyzed seasons. Looking at the spatial pattern (**Figure 2**), we find the weaker differences in
328 Norway, where soil moisture is barely limiting the stomatal conductance, while the larger differences
329 occur in the Mediterranean basin (i.e. Spain, South France, Italy, Greece and Turkey). In fact, in these
330 semi-arid regions the soil dries out quickly, especially during summer (**Figure 1**), and plants close
331 their stomata during the warmer hours of the day to prevent water loss, leading to a smaller amount of
332 O₃ entering the leaves and thus removed by vegetation. This process is well displayed during JAS in



333 the *SWC_10cm* simulation and to a lesser extent in the *SWC_40cm*, *SWC_1m* and *SWC_DYN*
334 simulations: specifically, in Southern Europe the upper soil layer (i.e. 10 cm) dries out faster than the
335 deeper ones during the warm and dry season, consequently, in the *SWC_10cm* simulation we find the
336 stronger limitation of soil moisture to stomatal conductance and the highest reduction in O₃ dry
337 deposition. In the other simulations we use a deeper rooting zone where plants can uptake water from
338 the soil; during summer these layers are generally moister than the shallow layer, thus the stomatal
339 conductance will be less limited by soil moisture and the vegetation removes a larger amount of O₃. In
340 addition to the larger stomatal conductance, during JAS, compared to AMJ, the higher leaf area index
341 (LAI) increases the surface resistance and thus the amount of O₃ removed from the surface layer; this
342 explains the larger O₃ dry deposition values found during summer. Overall, during the whole year the
343 amount of O₃ removed by dry deposition (sum of stomatal and non-stomatal deposition) integrated
344 over the only land points of domain is 8.568 TgO₃ in the *NO_SWC* simulation, 7.576 TgO₃ (-11.8%) in
345 the *SWC_10cm*, 7.618 TgO₃ (-11.1%) in the *SWC_40cm*, 7.617 TgO₃ (-11.1%) in the *SWC_1m*, and
346 7.693 TgO₃ (-10.2%) in the *SWC_DYN*.

347

348 3.3. Changes in O₃ concentration

349 As plants uptake atmospheric gases when stomata are open (Cieslik et al., 2009), changes in stomatal
350 behavior, and thus in dry deposition velocity, affect, in turn, the concentration of compounds
351 remaining in the lower atmosphere; **Figure 3** shows the mean percentage of change in O₃
352 concentration in the lowest model layer (20-25 meters in our case) between the reference simulation
353 (i.e. *NO_SWC*) and the other simulations. Unlike **Figure 2**, where we found a systematic negative
354 percentage of change in the amount of O₃ removed by dry deposition, **Figure 3** shows a systematic
355 positive percentage of change, i.e. a higher concentration of O₃ remaining in the atmosphere in the
356 simulations where soil moisture limits the stomatal conductance. In addition, the higher (i.e. more
357 negative) is the percentage of change of O₃ removed by deposition, the more is the concentration of O₃
358 remaining in the air: **Figure 3** clearly shows how the larger differences in surface O₃ concentration are
359 found during summer (JAS) in the *SWC_10cm* simulation, i.e. the experiment where soil moisture
360 plays the strongest limitation to stomatal conductance.

361 Similarly, the vertical mixing in surface layers, largely driven by wind and its interaction with
362 frictional drag at the surface (Monks et al., 2015), propagates the changes in O₃ concentration from the
363 surface layer to upper layers. **Figure 4** shows the O₃ anomaly between the reference simulation and the
364 simulations with soil water limitation, averaged over the plant growing season, i.e. April-September



365 (Anav et al., 2017); here we show only grid points with a significant change in O₃ concentration (t-test,
366 95% confidence), while we mask out points where the anomaly is not significant. The larger anomaly
367 in O₃ concentration (up to 4 ppb) is found in the whole Mediterranean basin for the *SWC_10cm*
368 simulation; interestingly, the anomaly is significant in almost all the grid points except Ireland and
369 Scotland, which are characterized by high soil moisture levels even during summer, and up to 800 hPa
370 where we find an O₃ anomaly larger than 1 ppb.

371

372 **3.4. Changes in the model performances**

373 As discussed above, the inclusion of soil water limitation to stomatal conductance leads to increased
374 O₃ concentration due to the reduced dry deposition rates; this clearly affects the model performances in
375 reproducing both the phase and amplitude of hourly O₃ concentration. Therefore, here we validate the
376 simulated O₃ against AirBase measurements.

377 **Figure 5** (upper panels) shows how the inclusion of the new parameterization leads to an increase of
378 model-data misfit during the temporal period April-September, being the percentage of change in
379 RMSE positive in all the ground stations. Overall, the mean RMSE (average over all the stations)
380 computed comparing hourly data is 17.8 ppb for the *NO_SWC* simulation, 19.5 ppb in the *SWC_10cm*
381 and *SWC_40cm*, and 19 ppb in the *SWC_1m* and *SWC_DYN* simulations.

382 Conversely, the new parameterization improves the model skills in reproducing the observed hourly
383 cycle (**Figure 5**, lower panels), being the percentage of change in correlation coefficient positive in all
384 the stations. Overall, the mean correlation computed from hourly data is 0.6 for the *NO_SWC*
385 simulation, 0.62 in the *SWC_10cm* and 0.64 in the *SWC_40cm*, *SWC_1m* and *SWC_DYN* simulations.

386

387 **4. Summary and conclusion**

388 In this study, we incorporated the soil moisture limitation into the dry deposition parameterization of
389 CHIMERE model and tested different hypotheses of water uptake by roots. Model simulations with the
390 improved parameterization indicate that O₃ dry deposition significantly declines when soil moisture
391 regulates the stomatal opening, particularly in Southern Europe where soil is close to the wilting point
392 during the dry summer. This mechanism, occurring within the soil, in turn, affects the concentration of
393 gases remaining into the lower atmosphere and, considering the vertical mixing in the boundary layer
394 and the long-lived species such as O₃, has an impact on O₃ concentration extending from the plants
395 canopy to the upper troposphere and decreasing with height; the influence on O₃ concentration then
396 quickly vanishes above the boundary layer, becoming no more significant above 650 hPa.



397 The analysis of simulated soil moisture suggests that actual water availability from April to September,
398 even in the Mediterranean sites, is higher than conventionally assumed; according to Allen et al.
399 (1998) and Martínez-Fernández et al. (2015), soil water content values corresponding to 40-50% of
400 total available water (TAW, FC-WP) often correspond to low stress conditions for cultivated plants. As
401 the stress threshold lowers with rooting depth (Allen et al 1998), it appears likely that the effect of
402 water deficit on forest vegetation is limited in these conditions. As in the modified DO₃SE model the
403 effect of soil water content on stomatal aperture is modeled as a linear function of SWC-WP (eq. 6), it
404 is possible that the actual reduction in stomatal conductance is overestimated for SWC values above
405 40-50% of TAW, i.e. the most common condition predicted by WRF in the April–September period
406 over the analyzed sites.

407 With the modified parameterization, CHIMERE shows increased bias in the prediction of surface
408 hourly O₃ concentrations across Europe with improved representation of the phase of the hourly cycle.
409 Therefore the new parameterization increases the well-known systematic overestimation of O₃
410 concentrations (e.g. Anav et al., 2016), which derives from initial and lateral boundary conditions
411 provided by the global chemistry-transport model LMDz-INCA that overestimate the observed
412 background concentrations (Terrenoire et al., 2015) as well as from bias in anthropogenic and biogenic
413 emissions.

414 It should also be noted that the model comparison to satellite retrievals is not obvious in this study: in
415 fact, here we mainly focus on O₃ changes in the boundary layer and lower troposphere, which
416 correspond to the part of the atmosphere where satellite data are not robust: as shown by Boynard et al.
417 (2016), the O₃ vertical profiles inversions begin to be efficient in the upper troposphere and in the
418 stratosphere, where our changes become to be negligible. Therefore, it would be largely uncertain to
419 extract the signal close to the surface and assess how much our different hypotheses improved the total
420 O₃ column. Similarly, the comparison with vertical soundings would display the simulated vertical
421 profiles very close each other.

422 Nevertheless our results can be used to improve the representation of soil moisture stress on vegetation
423 within chemistry transport models and to better describe the biogeochemical and biophysical feedbacks
424 between the complex soil-plant-atmosphere system in response to a changing climate toward warmer
425 and drier conditions. As the soil water uptake is mainly related to different rooting systems (Wu et al.,
426 2017), chemistry models would benefit from the inclusion of species-specific parameterizations which
427 ensure a water uptake depending on species-specific eco-hydrological properties. In general, plants in
428 water-limited regions can adapt to dry environments by accessing ground water (Craine et al., 2013)



429 based on the depth and density of the root system (Wu et al., 2017), while deep-rooted forests can take
430 up available water from deep soil during extreme drought events (Schwinning et al., 2005; Teuling et
431 al., 2010). Although some of these processes are already well resolved within land surface models used
432 by climate models, a better description of different rooting systems within the dry deposition schemes
433 might have significant implication for stomatal regulation and thus atmospheric chemistry. We also
434 believe that it is challenging for the near future the use of coupled land surface-chemistry models (e.g.
435 Anav et al., 2012) which allow to account for the different feedbacks between land surfaces and
436 atmospheric chemistry and physics.

437

438 *Code availability.* The model used in this study is freely available and provided under the GNU
439 general public license 4. The source code along with the corresponding technical documentation can be
440 obtained from the CHIMERE web site at <http://www.lmd.polytechnique.fr/chimere/>. All
441 measurement data are publicly available

442 *Competing interests.* The authors declare that they have no conflict of interest.

443

444 **Acknowledgements**

445 We thank the investigators and the teams managing the eddy-flux sites. We also acknowledge the
446 entire EMEP and AIRBASE staffs for providing ground based O₃ data and the EMEP/MSC-W team
447 for anthropogenic emissions database. The computing resources and the related technical support used
448 for this work have been provided by CRESCO/ENEA-GRID High Performance Computing
449 infrastructure and its staff (<http://www.cresco.enea.it>). CRESCO/ENEAGRID High Performance
450 Computing infrastructure is funded by ENEA, the Italian National Agency for New Technologies,
451 Energy and Sustainable Economic Development and by National and European research programs”.
452 Financial support was from the MITIMPACT project (INTERREG V A – Italy – France ALCOTRA).
453 This work was carried out within the IUFRO Task Force on Climate Change and Forest Health.

454

455

456

457

458 **References**

459 Ainsworth, E. A., Yendrek, C. R., Sitch, S., Collins, W. J., and Emberson, L. D.: The effects of
460 tropospheric ozone on net primary productivity and implications for climate change, *Annu Rev Plant*
461 *Biol*, 63, 637-661, 10.1146/annurev-arplant-042110-103829, 2012.

462

463 Allen, R. G., Pereira, L. S., Raes, D., and Smith, M.: Crop evapotranspiration-Guidelines for
464 computing crop water requirements-FAO Irrigation and drainage paper 56, FAO, Rome, 300, D05109,
465 1998.

466

467 Al-Shrafany, D., Rico-Ramirez, M. A., Han, D., and Bray, M.: Comparative assessment of soil
468 moisture estimation from land surface model and satellite remote sensing based on catchment water
469 balance, *Meteorological Applications*, 21, 521-534, 10.1002/met.1357, 2014.

470

471 Anav, A., Menut, L., Khvorostyanov, D., and Viovy, N.: A comparison of two canopy conductance
472 parameterizations to quantify the interactions between surface ozone and vegetation over Europe,
473 *Journal of Geophysical Research: Biogeosciences*, 117, n/a-n/a, 10.1029/2012jg001976, 2012.

474

475 Anav, A., De Marco, A., Proietti, C., Alessandri, A., Dell'Aquila, A., Cionni, I., Friedlingstein, P.,
476 Khvorostyanov, D., Menut, L., Paoletti, E., Sicard, P., Sitch, S., and Vitale, M.: Comparing
477 concentration-based (AOT40) and stomatal uptake (PODY) metrics for ozone risk assessment to
478 European forests, *Glob Chang Biol*, 22, 1608-1627, 10.1111/gcb.13138, 2016.

479

480 Anav, A., Liu, Q., De Marco, A., Proietti, C., Savi, F., Paoletti, E., and Piao, S.: The role of plant
481 phenology in stomatal ozone flux modeling, *Glob Chang Biol*, 10.1111/gcb.13823, 2017.

482

483 Aranda, I., Forner, A., Cuesta, B., and Valladares, F.: Species-specific water use by forest tree species:
484 from the tree to the stand, *Agricultural water management*, 114, 67-77, 2012.

485

486 Bolte, A., Czajkowski, T., and Kompa, T.: The north-eastern distribution range of European beech a
487 review, *Forestry*, 80, 413-429, 10.1093/forestry/cpm028, 2007.

488

489 Boynard, A., Hurtmans, D., Koukouli, M. E., Goutail, F., Bureau, J., Safieddine, S., Lerot, C., Hadji-
490 Lazaro, J., Wespes, C., Pommereau, J.-P., Pazmino, A., Zyrichidou, I., Balis, D., Barbe, A.,
491 Mikhailenko, S. N., Loyola, D., Valks, P., Van Roozendael, M., Coheur, P.-F., and Clerbaux, C.:
492 Seven years of IASI ozone retrievals from FORLI: validation with independent total column and
493 vertical profile measurements, *Atmospheric Measurement Techniques*, 9, 4327-4353, 10.5194/amt-9-
494 4327-2016, 2016.

495

496 Büker, P., Morrissey, T., Briolat, A., Falk, R., Simpson, D., Tuovinen, J. P., Alonso, R., Barth, S.,
497 Baumgarten, M., Grulke, N., Karlsson, P. E., King, J., Lagergren, F., Matyssek, R., Nunn, A., Ogaya,
498 R., Peñuelas, J., Rhea, L., Schaub, M., Uddling, J., Werner, W., and Emberson, L. D.: DO₃SE
499 modelling of soil moisture to determine ozone flux to forest trees, *Atmospheric Chemistry and Physics*,
500 12, 5537-5562, 10.5194/acp-12-5537-2012, 2012.

501

502 Canadell, J., Jackson, R., Ehleringer, J., Mooney, H., Sala, O., and Schulze, E.-D.: Maximum rooting
503 depth of vegetation types at the global scale, *Oecologia*, 108, 583-595, 1996.

504



- 505 Chen, F., and Dudhia, J.: Coupling an advanced land surface–hydrology model with the Penn State–
506 NCAR MM5 modeling system. Part I: Model implementation and sensitivity, *Monthly Weather*
507 *Review*, 129, 569–585, 2001.
508
- 509 Ciais, P., Reichstein, M., Viovy, N., Granier, A., Ogee, J., Allard, V., Aubinet, M., Buchmann, N.,
510 Bernhofer, C., Carrara, A., Chevallier, F., De Noblet, N., Friend, A. D., Friedlingstein, P., Grunwald,
511 T., Heinesch, B., Keronen, P., Knohl, A., Krinner, G., Loustau, D., Manca, G., Matteucci, G.,
512 Miglietta, F., Ourcival, J. M., Papale, D., Pilegaard, K., Rambal, S., Seufert, G., Soussana, J. F., Sanz,
513 M. J., Schulze, E. D., Vesala, T., and Valentini, R.: Europe-wide reduction in primary productivity
514 caused by the heat and drought in 2003, *Nature*, 437, 529–533, 10.1038/nature03972, 2005.
515
- 516 Cieslik, S., Omasa, K., and Paoletti, E.: Why and how terrestrial plants exchange gases with air, *Plant*
517 *Biol (Stuttg)*, 11 Suppl 1, 24–34, 10.1111/j.1438-8677.2009.00262.x, 2009.
518
- 519 Craine, J. M., Ocheltree, T. W., Nippert, J. B., Towne, E. G., Skibbe, A. M., Kembel, S. W., and
520 Fargione, J. E.: Global diversity of drought tolerance and grassland climate-change resilience, *Nature*
521 *Climate Change*, 3, 63–67, 10.1038/nclimate1634, 2012.
522
- 523 De Marco, A., Sicard, P., Fares, S., Tuovinen, J.-P., Anav, A., and Paoletti, E.: Assessing the role of
524 soil water limitation in determining the Phytotoxic Ozone Dose (PODY) thresholds, *Atmospheric*
525 *Environment*, 147, 88–97, 10.1016/j.atmosenv.2016.09.066, 2016.
526
- 527 Dee, D. P., Uppala, S. M., Simmons, A. J., Berrisford, P., Poli, P., Kobayashi, S., Andrae, U.,
528 Balsameda, M. A., Balsamo, G., Bauer, P., Bechtold, P., Beljaars, A. C. M., van de Berg, L., Bidlot, J.,
529 Bormann, N., Delsol, C., Dragani, R., Fuentes, M., Geer, A. J., Haimberger, L., Healy, S. B.,
530 Hersbach, H., Hólm, E. V., Isaksen, L., Kållberg, P., Köhler, M., Matricardi, M., McNally, A. P.,
531 Monge-Sanz, B. M., Morcrette, J. J., Park, B. K., Peubey, C., de Rosnay, P., Tavolato, C., Thépaut, J.
532 N., and Vitart, F.: The ERA-Interim reanalysis: configuration and performance of the data assimilation
533 system, *Quarterly Journal of the Royal Meteorological Society*, 137, 553–597, 10.1002/qj.828, 2011.
534
- 535 Domec, J. C., King, J. S., Noormets, A., Treasure, E., Gavazzi, M. J., Sun, G., and McNulty, S. G.:
536 Hydraulic redistribution of soil water by roots affects whole-stand evapotranspiration and net
537 ecosystem carbon exchange, *New Phytol*, 187, 171–183, 10.1111/j.1469-8137.2010.03245.x, 2010.
538
- 539 Dy, C. Y., and Fung, J. C. H.: Updated global soil map for the Weather Research and Forecasting
540 model and soil moisture initialization for the Noah land surface model, *Journal of Geophysical*
541 *Research: Atmospheres*, 121, 8777–8800, 10.1002/2015jd024558, 2016.
542
- 543 Eamus, D.: How does ecosystem water balance affect net primary productivity of woody ecosystems?,
544 *Functional Plant Biology*, 30, 187–205, 2003.
545
- 546 Emberson, L., Ashmore, M., Cambridge, H., Simpson, D., and Tuovinen, J.-P.: Modelling stomatal
547 ozone flux across Europe, *Environmental Pollution*, 109, 403–413, 2000.
548
- 549 Emberson, L. D., Büker, P., and Ashmore, M. R.: Assessing the risk caused by ground level ozone to
550 European forest trees: a case study in pine, beech and oak across different climate regions,
551 *Environmental Pollution*, 147, 454–466, 2007.
552



- 553 Folberth, G., Hauglustaine, D., Lathièrre, J., and Brocheton, F.: Interactive chemistry in the Laboratoire
554 de Météorologie Dynamique general circulation model: model description and impact analysis of
555 biogenic hydrocarbons on tropospheric chemistry, *Atmospheric Chemistry and Physics*, 6, 2319, 2006.
- 556 Gielen, B., Löw, M., Deckmyn, G., Metzger, U., Franck, F., Heerdt, C., Matyssek, R., Valcke, R., and
557 Ceulemans, R.: Chronic ozone exposure affects leaf senescence of adult beech trees: a chlorophyll
558 fluorescence approach, *Journal of Experimental Botany*, 58, 785-795, 2006.
- 559
- 560 Ginoux, P., Chin, M., Tegen, I., Prospero, J. M., Holben, B., Dubovik, O., and Lin, S. J.: Sources and
561 distributions of dust aerosols simulated with the GOCART model, *Journal of Geophysical Research:*
562 *Atmospheres*, 106, 20255-20273, 2001.
- 563
- 564 Granier, A., Huc, R., and Barigah, S.: Transpiration of natural rain forest and its dependence on
565 climatic factors, *Agricultural and forest meteorology*, 78, 19-29, 1996.
- 566
- 567 Granier, A., Reichstein, M., Bréda, N., Janssens, I., Falge, E., Ciais, P., Grünwald, T., Aubinet, M.,
568 Berbigier, P., and Bernhofer, C.: Evidence for soil water control on carbon and water dynamics in
569 European forests during the extremely dry year: 2003, *Agricultural and forest meteorology*, 143, 123-
570 145, 2007.
- 571
- 572 Greve, P., Warrach-Sagi, K., and Wulfmeyer, V.: Evaluating soil water content in a WRF-Noah
573 downscaling experiment, *Journal of Applied Meteorology and Climatology*, 52, 2312-2327, 2013.
- 574
- 575 Guehl, J., Aussenac, G., Bouachrine, J., Zimmermann, R., Pennes, J., Ferhi, A., and Grieu, P.:
576 Sensitivity of leaf gas exchange to atmospheric drought, soil drought, and water-use efficiency in some
577 Mediterranean *Abies* species, *Canadian Journal of Forest Research*, 21, 1507-1515, 1991.
- 578
- 579 Guenther, C.: Estimates of global terrestrial isoprene emissions using MEGAN (Model of Emissions of
580 Gases and Aerosols from Nature), *Atmospheric Chemistry and Physics*, 6, 2006.
- 581
- 582 Hardacre, C., Wild, O., and Emberson, L.: An evaluation of ozone dry deposition in global scale
583 chemistry climate models, *Atmospheric Chemistry and Physics*, 15, 6419-6436, 2015.
- 584
- 585 Hauglustaine, D., Hourdin, F., Jourdain, L., Filiberti, M. A., Walters, S., Lamarque, J. F., and Holland,
586 E.: Interactive chemistry in the Laboratoire de Météorologie Dynamique general circulation model:
587 Description and background tropospheric chemistry evaluation, *Journal of Geophysical Research:*
588 *Atmospheres*, 109, 2004.
- 589
- 590 Hibbard, K., Janetos, A., van Vuuren, D. P., Pongratz, J., Rose, S. K., Betts, R., Herold, M., and
591 Feddema, J. J.: Research priorities in land use and land-cover change for the Earth system and
592 integrated assessment modelling, *International Journal of Climatology*, 30, 2118-2128, 2010.
- 593
- 594 Hong, S.-Y., Dudhia, J., and Chen, S.-H.: A revised approach to ice microphysical processes for the
595 bulk parameterization of clouds and precipitation, *Monthly Weather Review*, 132, 103-120, 2004.
- 596
- 597 Hong, S.-Y., Noh, Y., and Dudhia, J.: A new vertical diffusion package with an explicit treatment of
598 entrainment processes, *Monthly weather review*, 134, 2318-2341, 2006.
- 599
- 600 Hoshika, Y., Katata, G., Deushi, M., Watanabe, M., Koike, T., and Paoletti, E.: Ozone-induced



- 601 stomatal sluggishness changes carbon and water balance of temperate deciduous forests, *Scientific*
602 *reports*, 5, srep09871, 2015.
- 603
- 604 Jackson, R., Canadell, J., Ehleringer, J., Mooney, H., Sala, O., and Schulze, E.: A global analysis of
605 root distributions for terrestrial biomes, *Oecologia*, 108, 389-411, 1996.
- 606
- 607 Jackson, R. B., Sperry, J. S., and Dawson, T. E.: Root water uptake and transport: using physiological
608 processes in global predictions, *Trends in plant science*, 5, 482-488, 2000.
- 609
- 610 Jarvis, P.: The interpretation of the variations in leaf water potential and stomatal conductance found in
611 canopies in the field, *Philosophical Transactions of the Royal Society of London B: Biological*
612 *Sciences*, 273, 593-610, 1976.
- 613
- 614 Kain, J. S.: The Kain–Fritsch convective parameterization: an update, *Journal of Applied Meteorology*,
615 43, 170-181, 2004.
- 616
- 617 Karlsson, P. E., Klingberg, J., Engardt, M., Andersson, C., Langner, J., Karlsson, G. P., and Pleijel, H.:
618 Past, present and future concentrations of ground-level ozone and potential impacts on ecosystems and
619 human health in northern Europe, *Science of The Total Environment*, 576, 22-35, 2017.
- 620
- 621 Karnosky, D., Percy, K. E., Xiang, B., Callan, B., Noormets, A., Mankovska, B., Hopkin, A., Sober, J.,
622 Jones, W., and Dickson, R.: Interacting elevated CO₂ and tropospheric O₃ predisposes aspen (*Populus*
623 *tremuloides* Michx.) to infection by rust (*Melampsora medusae* f. sp. *tremuloidae*), *Global Change*
624 *Biology*, 8, 329-338, 2002.
- 625
- 626 Klingberg, J., Engardt, M., Karlsson, P. E., Langner, J., and Pleijel, H.: Declining ozone exposure of
627 European vegetation under climate change and reduced precursor emissions, *Biogeosciences*, 11,
628 5269-5283, 2014.
- 629
- 630 Lattuati, M.: Impact des émissions européennes sur le bilan de l'ozone troposphérique à l'interface de
631 l'Europe et de l'Atlantique nord: apport de la modélisation lagrangienne et des mesures en altitude, Phd
632 thesis, Université P.M.Curie, Paris, France, 1997.
- 633
- 634 Loveland, T. R., Reed, B. C., Brown, J. F., Ohlen, D. O., Zhu, Z., Yang, L., and Merchant, J. W.:
635 Development of a global land cover characteristics database and IGBP DISCover from 1 km AVHRR
636 data, *International Journal of Remote Sensing*, 21, 1303-1330, 2000.
- 637
- 638 Mailler, S., Menut, L., Di Sarra, A., Becagli, S., Di Iorio, T., Bessagnet, B., Briant, R., Formenti, P.,
639 Doussin, J.-F., and Gómez-Amo, J.: On the radiative impact of aerosols on photolysis rates:
640 comparison of simulations and observations in the Lampedusa island during the ChArMEx/ADRI-MED
641 campaign, *Atmospheric Chemistry and Physics*, 16, 1219-1244, 2016.
- 642
- 643 Mailler, S., Menut, L., Khvorostyanov, D., Valari, M., Couvidat, F., Siour, G., Turquety, S., Briant, R.,
644 Tuccella, P., and Bessagnet, B.: CHIMERE-2017: from urban to hemispheric chemistry-transport
645 modeling, *Geoscientific Model Development*, 10, 2397, 2017.
- 646
- 647 Martínez-Fernández, J., González-Zamora, A., Sánchez, N., and Gumuzzio, A.: A soil water based
648 index as a suitable agricultural drought indicator, *Journal of Hydrology*, 522, 265-273, 2015.



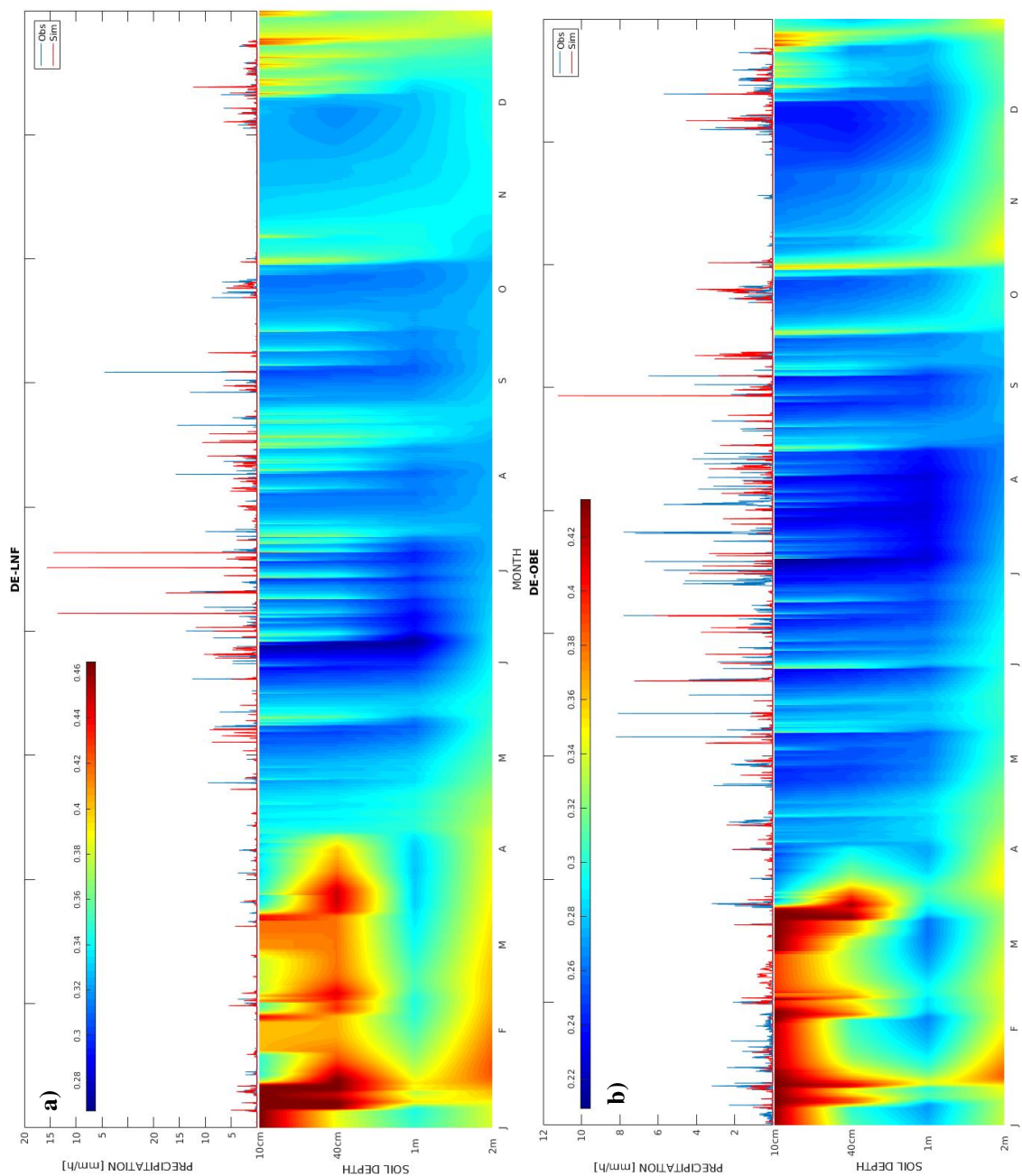
- 649
650 Martínez-Ferri, E., Balaguer, L., Valladares, F., Chico, J., and Manrique, E.: Energy dissipation in
651 drought-avoiding and drought-tolerant tree species at midday during the Mediterranean summer, *Tree*
652 *Physiology*, 20, 131-138, 2000.
- 653
654 Menut, L., Bessagnet, B., Khvorostyanov, D., Beekmann, M., Blond, N., Colette, A., Coll, I., Curci,
655 G., Foret, G., and Hodzic, A.: CHIMERE 2013: a model for regional atmospheric composition
656 modelling, *Geoscientific Model Development*, 6, 981-1028, 2014.
- 657
658 Mills, G., Pleijel, H., Braun, S., Büker, P., Bermejo, V., Calvo, E., Danielsson, H., Emberson, L.,
659 Fernández, I. G., and Grünhage, L.: New stomatal flux-based critical levels for ozone effects on
660 vegetation, *Atmospheric Environment*, 45, 5064-5068, 2011.
- 661
662 Mlawer, E. J., Taubman, S. J., Brown, P. D., Iacono, M. J., and Clough, S. A.: Radiative transfer for
663 inhomogeneous atmospheres: RRTM, a validated correlated-k model for the longwave, *Journal of*
664 *Geophysical Research: Atmospheres*, 102, 16663-16682, 1997.
- 665
666 Monks, P. S., Archibald, A., Colette, A., Cooper, O., Coyle, M., Derwent, R., Fowler, D., Granier, C.,
667 Law, K. S., and Mills, G.: Tropospheric ozone and its precursors from the urban to the global scale
668 from air quality to short-lived climate forcer, *Atmospheric Chemistry and Physics*, 15, 8889-8973,
669 2015.
- 670
671 Myhre, G., Shindell, D., Bréon, F.-M., Collins, W., Fuglestedt, J., Huang, J., Koch, D., Lamarque, J.-
672 F., Lee, D., and Mendoza, B.: Anthropogenic and natural radiative forcing, *Climate change*, 423, 658-
673 740, 2013.
- 674
675 Pataki, D. E., Oren, R., and Smith, W. K.: Sap flux of co-occurring species in a western subalpine
676 forest during seasonal soil drought, *Ecology*, 81, 2557-2566, 2000.
- 677
678 Pataki, D., and Oren, R.: Species differences in stomatal control of water loss at the canopy scale in a
679 mature bottomland deciduous forest, *Advances in Water Resources*, 26, 1267-1278, 2003.
- 680
681 Picon, C., Guehl, J., and Ferhi, A.: Leaf gas exchange and carbon isotope composition responses to
682 drought in a drought-avoiding (*Pinus pinaster*) and a drought-tolerant (*Quercus petraea*) species under
683 present and elevated atmospheric CO₂ concentrations, *Plant, Cell & Environment*, 19, 182-190, 1996.
- 684
685 Reichstein, M., Ciais, P., Papale, D., Valentini, R., Running, S., Viovy, N., Cramer, W., Granier, A.,
686 Ogee, J., and Allard, V.: Reduction of ecosystem productivity and respiration during the European
687 summer 2003 climate anomaly: a joint flux tower, remote sensing and modelling analysis, *Global*
688 *Change Biology*, 13, 634-651, 2007.
- 689
690 Reynolds, J. F., Smith, D. M. S., Lambin, E. F., Turner, B., Mortimore, M., Batterbury, S. P.,
691 Downing, T. E., Dowlatabadi, H., Fernández, R. J., and Herrick, J. E.: Global desertification: building
692 a science for dryland development, *science*, 316, 847-851, 2007.
- 693
694 Schaake, J. C., Koren, V. I., Duan, Q. Y., Mitchell, K., and Chen, F.: Simple water balance model for
695 estimating runoff at different spatial and temporal scales, *Journal of Geophysical Research:*
696 *Atmospheres*, 101, 7461-7475, 1996.

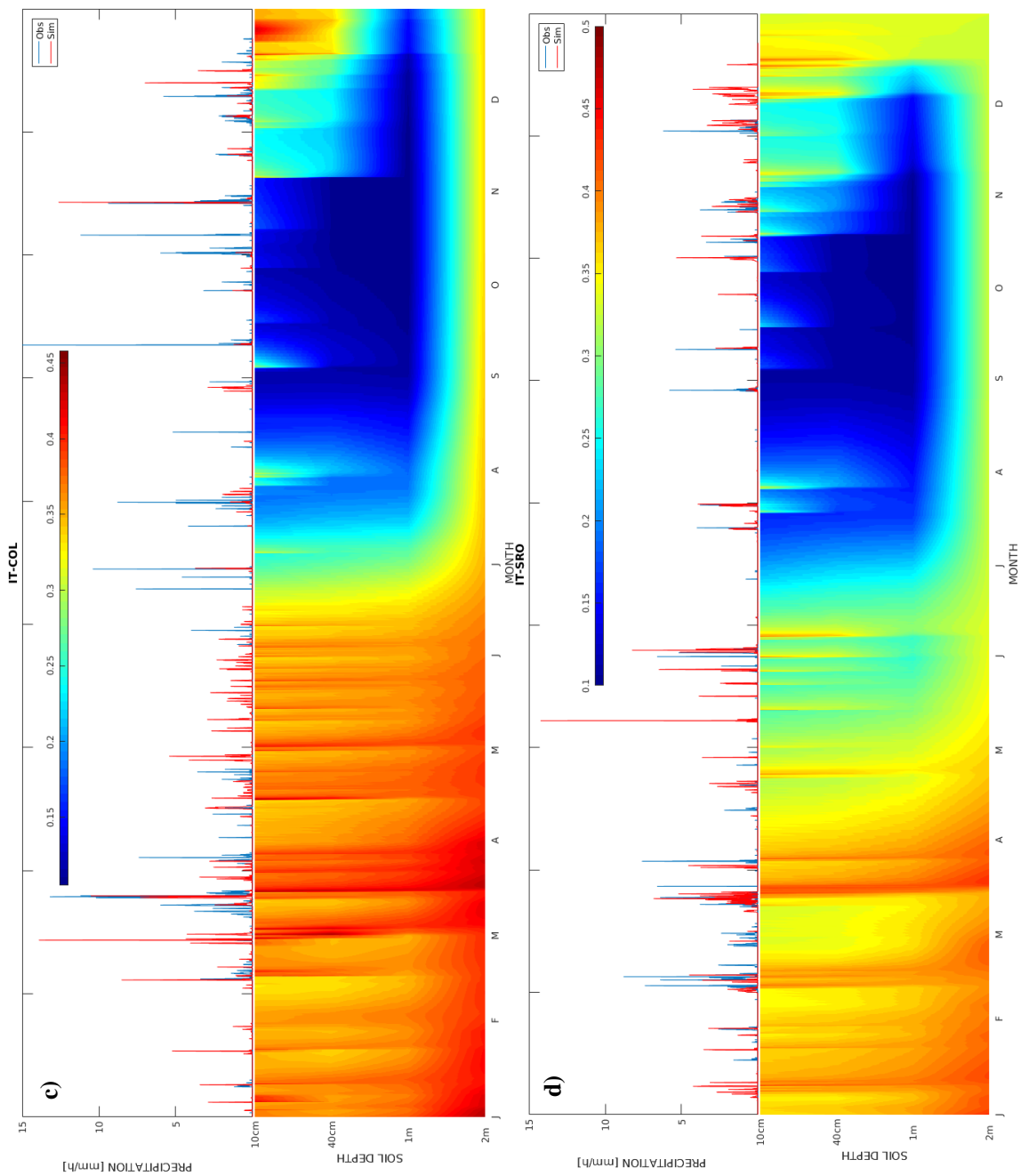


- 697 Schenk, H. J., and Jackson, R. B.: Rooting depths, lateral root spreads and below-ground/above-ground
698 allometries of plants in water-limited ecosystems, *Journal of Ecology*, 90, 480-494, 2002.
699
- 700 Schwinning, S., Starr, B. I., and Ehleringer, J. R.: Summer and winter drought in a cold desert
701 ecosystem (Colorado Plateau) part I: effects on soil water and plant water uptake, *Journal of Arid*
702 *Environments*, 60, 547-566, 2005.
703
- 704 Seinfeld, J. H., and Pandis, S. N.: *Atmospheric chemistry and physics: from air pollution to climate*
705 *change*, John Wiley & Sons, 2016.
706
- 707 Sertel, E., Robock, A., and Ormeci, C.: Impacts of land cover data quality on regional climate
708 simulations, *International Journal of Climatology*, 30, 1942-1953, 2010.
709
- 710 Shindell, D. T., Faluvegi, G., Koch, D. M., Schmidt, G. A., Unger, N., and Bauer, S. E.: Improved
711 attribution of climate forcing to emissions, *Science*, 326, 716-718, 2009.
712
- 713 Shindell, D. T., Lamarque, J.-F., Schulz, M., Flanner, M., Jiao, C., Chin, M., Young, P., Lee, Y. H.,
714 Rotstayn, L., and Mahowald, N.: Radiative forcing in the ACCMIP historical and future climate
715 simulations, *Atmospheric Chemistry and Physics*, 13, 2939-2974, 2013.
716
- 717 Sicard, P., De Marco, A., Dalstein-Richier, L., Tagliaferro, F., Renou, C., and Paoletti, E.: An
718 epidemiological assessment of stomatal ozone flux-based critical levels for visible ozone injury in
719 Southern European forests, *Science of the Total Environment*, 541, 729-741, 2016.
720
- 721 Simpson, D., Ashmore, M. R., Emberson, L., and Tuovinen, J.-P.: A comparison of two different
722 approaches for mapping potential ozone damage to vegetation. A model study, *Environmental*
723 *Pollution*, 146, 715-725, 2007.
724
- 725 Simpson, D., Benedictow, A., Berge, H., Bergström, R., Emberson, L. D., Fagerli, H., Flechard, C. R.,
726 Hayman, G. D., Gauss, M., and Jonson, J. E.: The EMEP MSC-W chemical transport model—technical
727 description, *Atmospheric Chemistry and Physics*, 12, 7825-7865, 2012.
728
- 729 Sitch, S., Cox, P., Collins, W., and Huntingford, C.: Indirect radiative forcing of climate change
730 through ozone effects on the land-carbon sink, *Nature*, 448, 791-794, 2007.
731
- 732 Skamarock, W. C., and Klemp, J. B.: A time-split nonhydrostatic atmospheric model for weather
733 research and forecasting applications, *Journal of Computational Physics*, 227, 3465-3485, 2008.
734
- 735 Terrenoire, E., Bassagnet, B., Rouil, L., Tognet, F., Pirovano, G., Létinois, L., Beauchamp, M.,
736 Colette, A., Thunis, P., and Amann, M.: High-resolution air quality simulation over Europe with the
737 chemistry transport model CHIMERE, *Geoscientific Model Development*, 8, 21-42, 2015.
738
- 739 Teuling, A. J., Seneviratne, S. I., Stöckli, R., Reichstein, M., Moors, E., Ciais, P., Luysaert, S., Van
740 Den Hurk, B., Ammann, C., and Bernhofer, C.: Contrasting response of European forest and grassland
741 energy exchange to heatwaves, *Nature Geoscience*, 3, 722-727, 2010.
742
- 743 Tuovinen, J.-P., Ashmore, M., Emberson, L., and Simpson, D.: Testing and improving the EMEP
744 ozone deposition module, *Atmospheric Environment*, 38, 2373-2385, 2004.



- 745 Tuovinen, J.-P., Emberson, L., and Simpson, D.: Modelling ozone fluxes to forests for risk assessment:
746 status and prospects, *Annals of Forest Science*, 66, 1-14, 2009.
747
- 748 Vestreng, V., Ntziachristos, L., Semb, A., Reis, S., Isaksen, I. S., and Tarrasón, L.: Evolution of NO_x
749 emissions in Europe with focus on road transport control measures, *Atmospheric Chemistry and*
750 *Physics*, 9, 1503-1520, 2009.
751
- 752 Wesely, M.: Parameterization of surface resistances to gaseous dry deposition in regional-scale
753 numerical models, *Atmospheric Environment (1967)*, 23, 1293-1304, 1989.
754
- 755 Vinceti, B., Paoletti, E., and Wolf, U.: Analysis of soil, roots and mycorrhizae in a Norway spruce
756 declining forest, *Chemosphere*, 36, 937-942, 1998.
757
- 758 Wild, O., Zhu, X., and Prather, M. J.: Fast-J: Accurate simulation of in-and below-cloud photolysis in
759 tropospheric chemical models, *Journal of Atmospheric Chemistry*, 37, 245-282, 2000.
760
- 761 Wittig, V. E., Ainsworth, E. A., Naidu, S. L., Karnosky, D. F., and Long, S. P.: Quantifying the impact
762 of current and future tropospheric ozone on tree biomass, growth, physiology and biochemistry: a
763 quantitative meta-analysis, *Global Change Biology*, 15, 396-424, 2009.
764
- 765 Wu, X., Liu, H., Li, X., Ciais, P., Babst, F., Guo, W., Zhang, C., Magliulo, V., Pavelka, M., and Liu,
766 S.: Differentiating drought legacy effects on vegetation growth over the temperate Northern
767 Hemisphere, *Global Change Biology*, 2017.
768
- 769 Zhu, Z., Bi, J., Pan, Y., Ganguly, S., Anav, A., Xu, L., Samanta, A., Piao, S., Nemani, R. R., and
770 Myneni, R. B.: Global data sets of vegetation leaf area index (LAI) 3g and Fraction of
771 Photosynthetically Active Radiation (FPAR) 3g derived from Global Inventory Modeling and
772 Mapping Studies (GIMMS) Normalized Difference Vegetation Index (NDVI3g) for the period 1981 to
773 2011, *Remote sensing*, 5, 927-948, 2013.
774
- 775 Zhu, Z., Piao, S., Myneni, R. B., Huang, M., Zeng, Z., Canadell, J. G., Ciais, P., Sitch, S.,
776 Friedlingstein, P., and Arneeth, A.: Greening of the Earth and its drivers, *Nature climate change*, 6, 791-
777 795, 2016.
778 .
779







785 **Figure 1.** Comparison of hourly precipitation simulated by WRF with observations collected at four measurement sites along with changes in the
786 vertical distribution of soil moisture ($\text{m}^3 \text{m}^{-3}$) during the year.
787
788
789
790
791

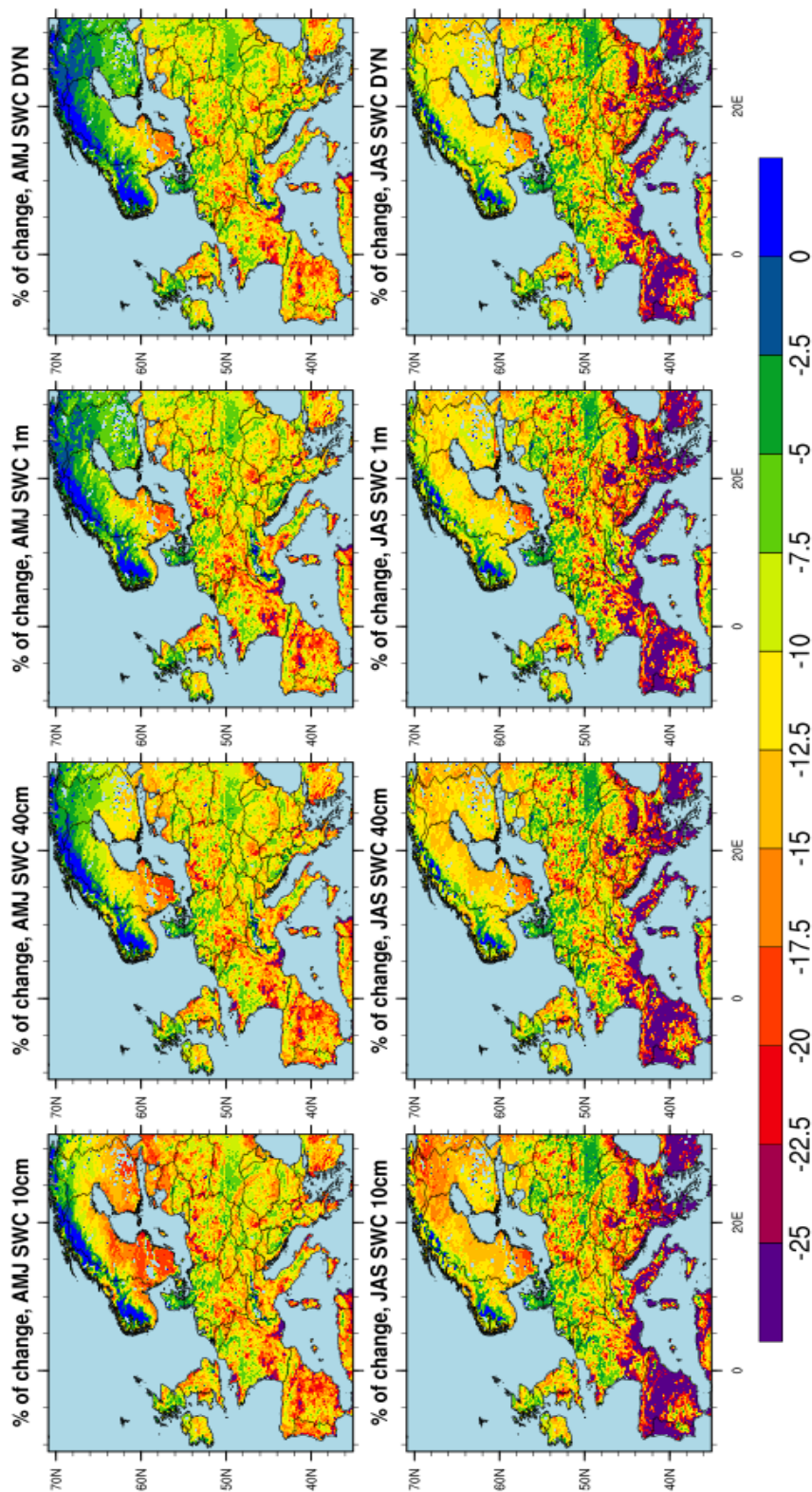


Figure 2. Percentage of change in the amount of O₃ removed by dry deposition over the land points (sea points are masked) computed in the time periods April-May-June (AMJ) and July-August-September (JAS). The percentage of change is defined as: $[(\text{Sim}-\text{Ref})/\text{Ref}]*100$, where Ref is the *NO_SWC* simulation and Sim represents the other simulations. A percentage of change of 25% corresponds to about 6 kg O₃ m⁻² d⁻¹.

792
 793
 794
 795
 796
 797
 798

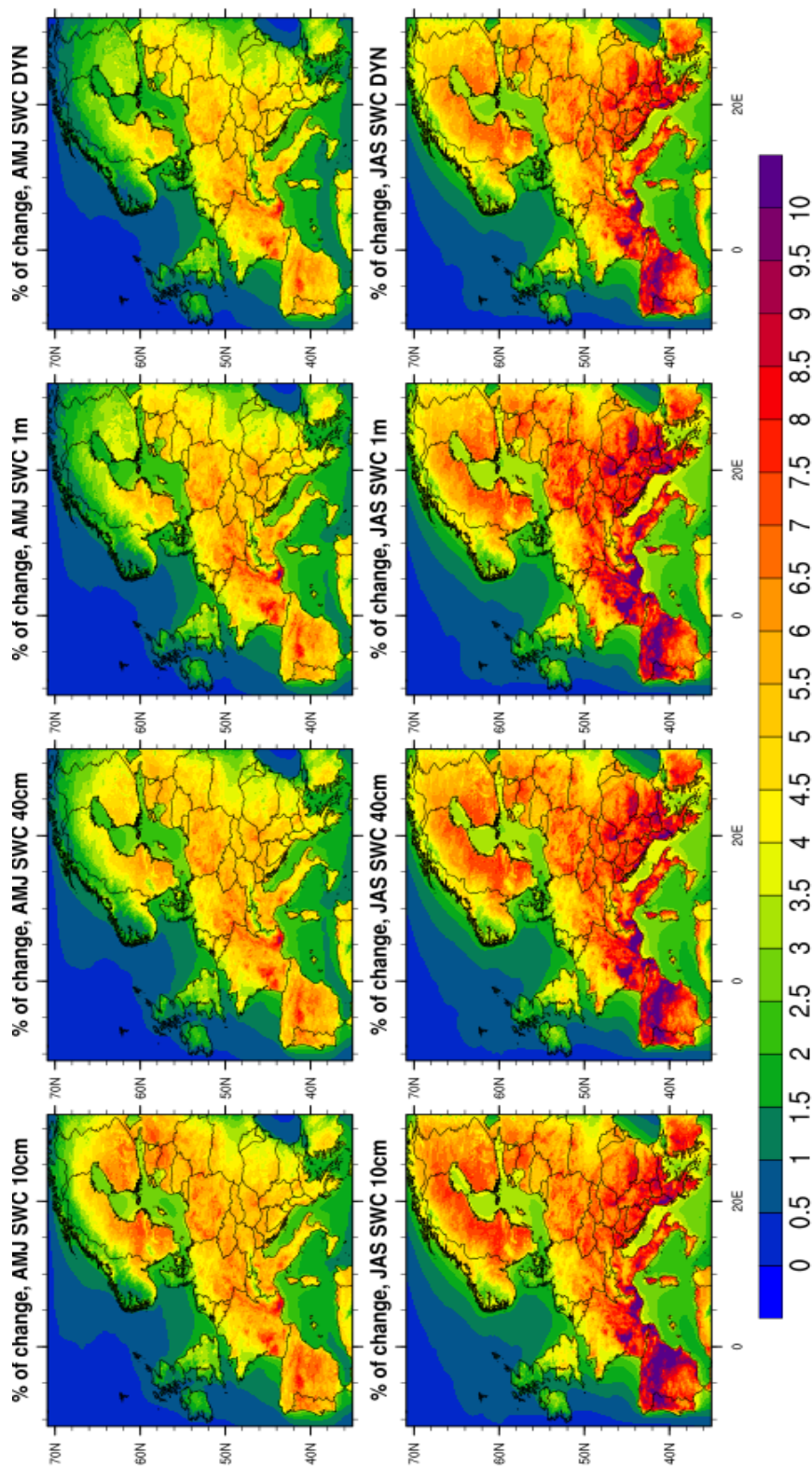


Figure 3. Percentage of change in surface O₃ concentration (absolute values are given in Figure 4).

799
800
801
802
803
804

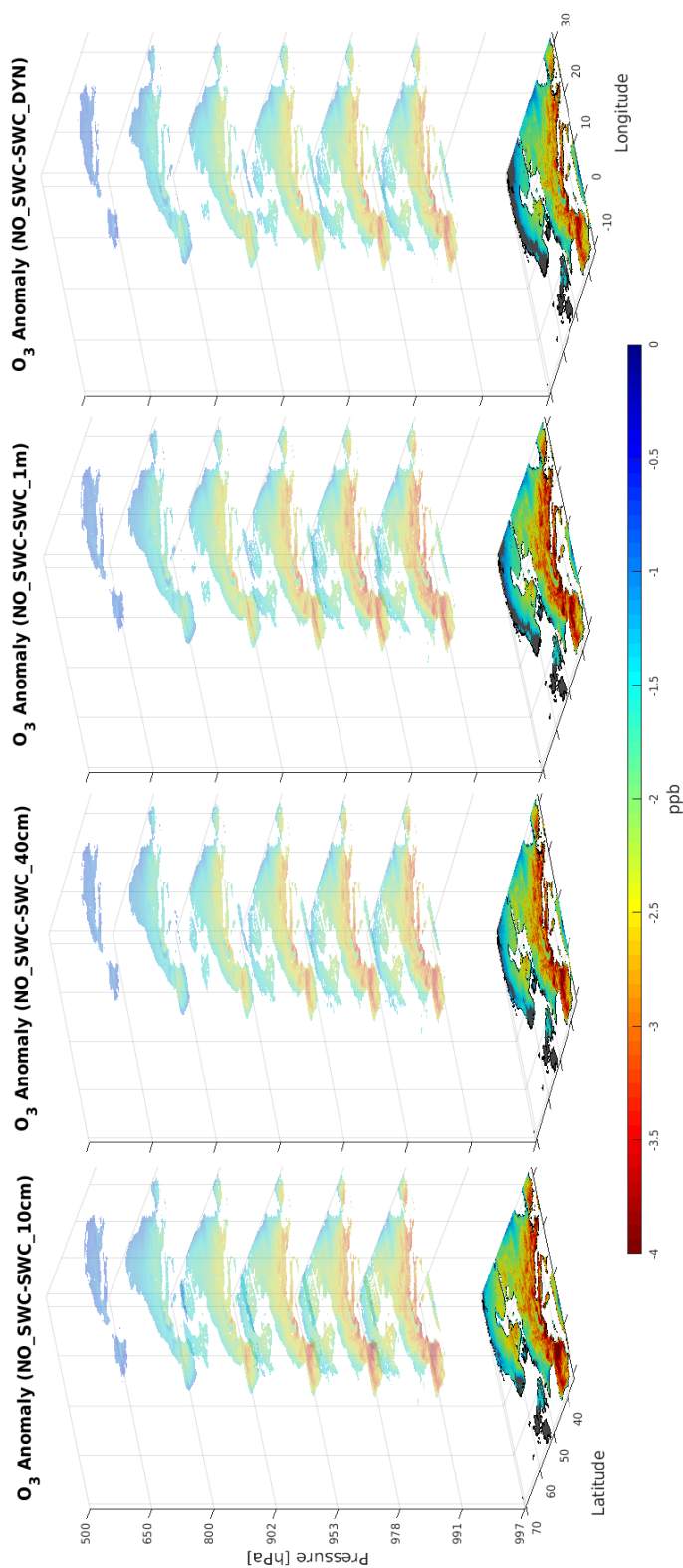


Figure 4. Vertical anomaly in O₃ concentration computed during the time period April-September.

805
806
807
808
809
810
811

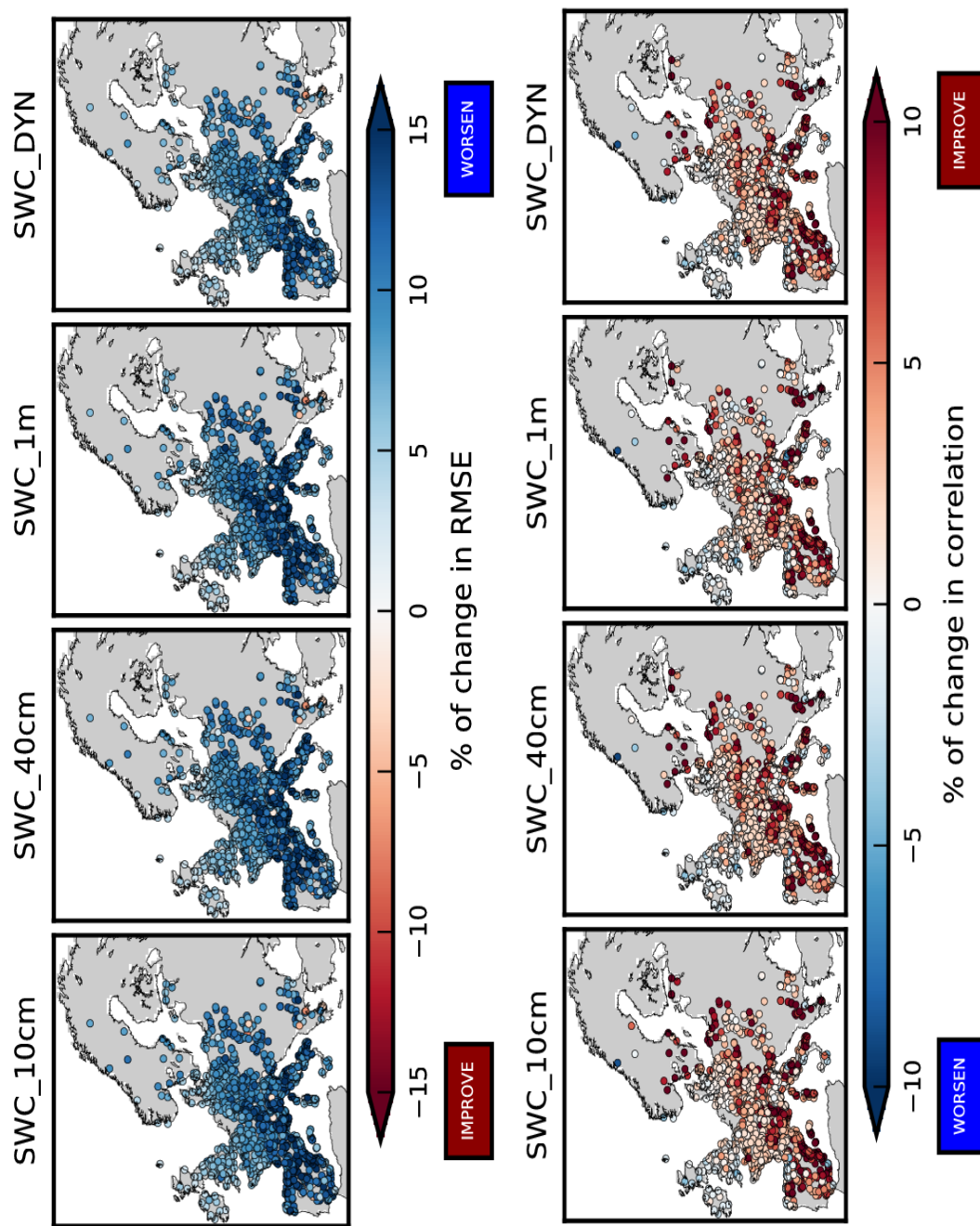


Figure 5. Percentage of change in RMSE (upper panels) and correlation coefficient (lower panels) computed using hourly data in the time period April-September. The reference simulation is *NO_SWC*.

812

813

814

815